JOURNAL OF SCIENCE TECHNOLOGY AND EDUCATION 14(3), SEPTEMBER, 2026
E-ISSN: 3093-0898, PRINT ISSN: 2277-0011; Journal homepage: www.atbufstejoste.com

Simulation and Experimental Validation of a 1.5 kW Three-Phase Squirrel-Cage Induction Motor using Finite Element Analysis

Onwe Peter Daffin, Patrick Otubu Odu, Lehiowo Obojor-Ogar
Department of Electrical and Electronic Engineering, University of Calabar, Nigeria

ABSTRACT

This study examines the rated-load performance of a 1.5 kW, three-phase squirrel-cage induction motor using finite element analysis and experimental measurements. The motor was modelled in ANSYS Motor-CAD using its geometry, winding arrangement, material properties, and rated operating conditions. The simulation was used to study the motor response during starting and at steady state. MATLAB was used to process and plot the simulation results. The parameters considered were the three-phase stator currents, electromagnetic torque, rotor speed, torque-speed characteristic, efficiency, and power factor. Experimental measurements were taken from the motor at a supply voltage of 380 V and compared with the simulation results. The simulated RMS currents for Phases A, B, and C were 3.734 A, 3.737 A, and 3.743 A, respectively, giving an average current of 3.738 A. The simulated electromagnetic torque was 10.014 Nm, while the steady-state speed was 1429 rpm. At 380 V, the measured currents were 3.70 A, 3.68 A, and 3.86 A for Phases A, B, and C, respectively, with an average current of 3.75 A and a measured speed of 1427 rpm. The differences between the simulated and measured currents were 0.92%, 1.55%, and 3.03%, respectively, while the difference in speed was 0.21%. The small differences between the measured and simulated values show that the Motor-CAD model gives a reasonable representation of the motor's electromagnetic performance at rated load.

ARTICLE INFO
Article History
Received, May, 2026
Received in revised form, May, 2026
Accepted, August, 2026
Published online, September, 2026

KEYWORDS
Squirrel-Cage Induction Motor; Finite Element Analysis; Motor-CAD; Rated Load; Electromagnetic Torque; Experimental Validation; MATLAB

INTRODUCTION

Three-phase squirrel-cage induction motors are widely used in industries and commercial facilities because they are simple in construction, reliable, durable, and require relatively little maintenance [10]–[13]. They are used in equipment such as pumps, fans, compressors, conveyors, and machine tools, where continuous and reliable operation is required. Knowing how an induction motor performs under operating conditions is important when assessing its performance. Analytical and equivalent-circuit methods are commonly used to estimate motor performance, but these methods make some assumptions about the magnetic field, leakage flux, rotor geometry, and interaction between the stator and rotor [11]–[13]. Such assumptions can limit the level of detail that can be obtained from the analysis.

Finite element analysis (FEA) can be used to obtain more detailed information about the electromagnetic behaviour of an induction motor. It allows the magnetic conditions in the stator, air gap, and rotor to be examined and provides quantities such as electromagnetic torque, current density, magnetic flux density, and losses [1], [14]. Abunike *et al.* [1] used FEA to study the steady-state and dynamic behaviour of an induction motor, while Deshmukh *et al.* [14] used FEA to assess the performance of a three-phase squirrel-cage induction motor.

Several other studies have used numerical methods to examine the performance of induction motors under different operating

Corresponding author: Onwe Peter Daffin
peteronwe@unical.edu.ng
Department of Electrical and Electronic Engineering, University of Calabar, Nigeria.

JOURNAL OF SCIENCE TECHNOLOGY AND EDUCATION 14(3), SEPTEMBER, 2026
E-ISSN: 3093-0898, PRINT ISSN: 2277-0011; Journal homepage: www.atbufstejoste.com

conditions [2]–[9]. These studies show that simulation can be useful for studying motor performance. However, simulation results need to be compared with measurements from an actual motor to determine how well the model represents the real machine.

In this study, a 1.5 kW three-phase squirrel-cage induction motor was modelled in ANSYS Motor-CAD and its performance was examined at rated load. The study considers the three-phase stator currents, electromagnetic torque, rotor speed, efficiency, and power factor. The simulation results were compared with measurements taken from the actual motor at a supply voltage of 380 V.

The main aim of the study is to determine how closely the Motor-CAD results agree with the measured performance of the motor at rated load. This comparison provides a basis for assessing the accuracy of the developed motor model.

MATHEMATICAL MODELLING OF THE INDUCTION MOTOR

Electrical and electromagnetic model

The mathematical representation of a three-phase induction motor can be expressed using electrical and mechanical relationships. The electrical behaviour is governed by the stator and rotor voltage equations, while the mechanical behaviour is determined by the interaction between electromagnetic torque, load torque, mechanical losses, and rotor inertia [11], [12].

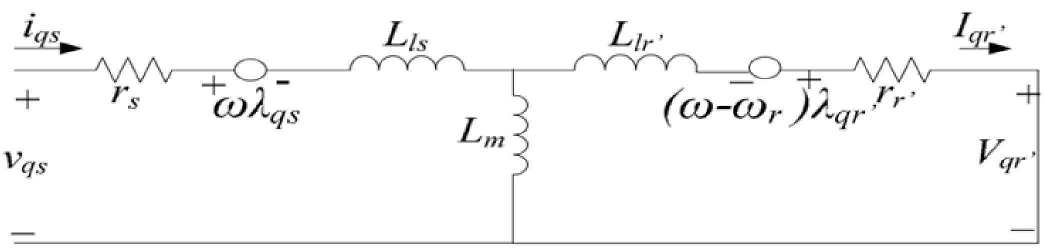

Figure. 1: Q-axis equivalent circuit of an induction motor

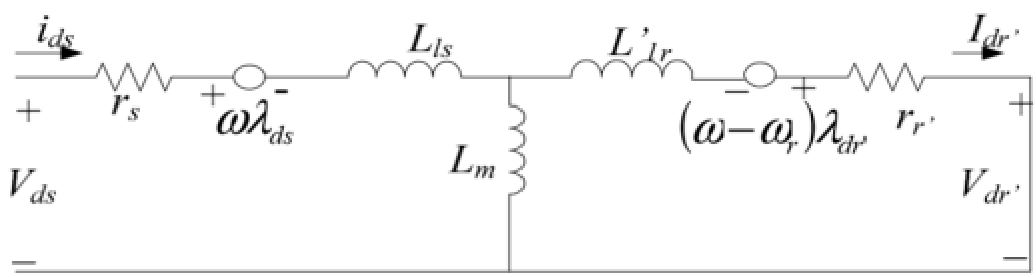

Figure. 2: D-axis equivalent circuit of an induction motor

Figure. 3: O-axis equivalent circuit of an induction motor

Corresponding author: Onwe Peter Daffin
peteronwe@unical.edu.ng
Department of Electrical and Electronic Engineering, University of Calabar, Nigeria.

JOURNAL OF SCIENCE TECHNOLOGY AND EDUCATION 14(3), SEPTEMBER, 2026
E-ISSN: 3093-0898, PRINT ISSN: 2277-0011; Journal homepage: www.atbufstejoste.com

The D-Q Voltage Equations are obtained as

$$V_{qs} = r_s i_{qs} + \omega\lambda_{ds} + \frac{d}{dt}\lambda_{qs} \quad 1$$

$$V_{ds} = r_s i_{ds} + \omega\lambda_{qs} + \frac{d}{dt}\lambda_{ds} \quad 2$$

The electromagnetic torque equation can be expressed as

$$T_e = \frac{3p}{2}(\lambda_{ds} i_{qs} - \lambda_{qs} i_{ds}) \quad 3$$

The balance between electromagnetic torque, load torque, and rotor inertia governs the mechanical behaviour of the induction motor. The equation governing the rotor motion is given by [12]:

$$J\frac{d\omega_r}{dt} = T_e - T_l - T_b \quad 4$$

Where T_e is the electromagnetic torque, T_l is the load torque, T_b is the mechanical loss torque due to friction and windage, J is the combined rotor and load inertia, and ω_r is the rotor angular speed.

The rated shaft torque is obtained from the rated mechanical output power and rated angular speed [10]–[13]:

$$T_n = \frac{P_n}{\omega_n} \quad 5$$

Where T_n is the rated torque, P_n is the rated mechanical output power, and ω_n is the rated angular speed. The rated angular speed is obtained from the rated rotational speed as:

$$\omega_n = \frac{2\pi N_n}{60} \quad 6$$

where N_n is the rated speed in revolutions per minute (rpm).
The slip of the induction motor is given by:

$$s = \frac{N_{s-} N_r}{N_s} \quad 7$$

where N_s is the synchronous speed and N_r is the rotor speed. Slip is necessary for electromagnetic torque production in an induction motor [10]–[13].

For a four-pole, 50 Hz induction motor,

$$N_s = \frac{120f}{N_s} \quad 8$$

Where f is the supply frequency and p is the number of poles.
Slip is essential to induction motor operation because relative motion between the rotating magnetic field and rotor is required to induce rotor current and produce electromagnetic torque [10]–[13].

The efficiency of the induction motor is defined as the ratio of the useful mechanical output power to the electrical input power [10]–[13]:

$$\eta = \frac{P_{out}}{P_{in}} \text{ x } 100\% \quad 9$$

where P_{out} is the mechanical output power and P_{in} is the electrical input power.
Alternatively,

$$\eta = \frac{P_{out}}{P_{out}+P_{loss}} \text{ x } 100\% \quad 10$$

The total machine losses include copper, iron, mechanical, and other losses:

$$P_{loss} = P_{cu} + P_{iron} + P_{mv} + P_{stray} \quad 11$$

This relationship was used in interpreting the efficiency characteristics obtained from Motor-CAD.

Motor Specification and Finite Element Model

The motor investigated is a 1.5 kW, three-phase squirrel-cage induction motor. The principal machine parameters used in the finite element model are presented in Table 1.

Table 1: Motor specification and geometry

Parameters	Value
Rated power	1.5 kW
Rated voltage	380 V
Rated current	3.83 A
Rated speed	1430 rpm
Frequency	50 Hz
Pole number	4
Slot number	24
Stator lamination diameter	170mm
Stator bore	98.6mm
Tooth width	10mm
Rotor bars	34
Slot depth	25mm

Corresponding author: Onwe Peter Daffin
peteronwe@unical.edu.ng
Department of Electrical and Electronic Engineering, University of Calabar, Nigeria.

JOURNAL OF SCIENCE TECHNOLOGY AND EDUCATION 14(3), SEPTEMBER, 2026
E-ISSN: 3093-0898, PRINT ISSN: 2277-0011; Journal homepage: www.atbufstejoste.com

Parameters	Value
Yoke thickness	12mm
Airgap	1mm
Shaft diameter	28mm
Rotor diameter	96.6mm
Rotor tooth width	4mm
Bar opening	1.5mm
Bar depth	10mm

The parameters listed in Table 1 were used to construct the motor geometry and define the electromagnetic model in Motor-CAD.

Finite Element Formulation

Finite element analysis of electrical machines is based on Maxwell's equations, which describe the interaction between electric and magnetic fields [1], [12], [14]. For the electromagnetic analysis of the induction motor, the relevant field relationships include Gauss's law for magnetism and Ampère's law. In the quasi-static electromagnetic formulation used for machine analysis, the displacement-current term can be neglected, giving

$$\nabla . B = 0 \quad 12$$

And

$$\nabla \times H = J \quad 13$$

Where B is the magnetic flux density, H is the magnetic field intensity, and is the current density. The magnetic flux density can be expressed in terms of the magnetic vector potential A as

$$B = \nabla \times A \quad 14$$

The magnetic vector potential formulation enables the electromagnetic field distribution within the stator, air gap, and rotor regions to be determined numerically. The material relationship

$$B = \mu H \quad 15$$

is used to account for the magnetic properties of the machine materials. In the present study, the finite element model incorporates the nonlinear magnetic characteristics of the electrical steel through the FEA saturation model.

The resulting electromagnetic field problem was solved numerically in ANSYS Motor-CAD using the defined motor geometry, winding configuration, material properties, supply voltage, frequency, and rated-load operating condition. The solution was used to obtain the phase currents, electromagnetic torque, rotor speed, efficiency, power factor, and magnetic field quantities required for the performance assessment.

The finite element modelling procedure consisted of:

1. development of the motor geometry;
2. definition of the stator winding configuration;
3. assignment of material properties to the stator, rotor, winding, and shaft;
4. specification of the rated operating conditions;
5. generation of the finite element mesh;
6. solution of the electromagnetic field problem; and
7. extraction and post-processing of the required rated-load performance parameters.

This approach is consistent with established FEA-based induction motor analysis reported in the literature [1], [14]. Figure 4 and table 2 shows the developed geometry of the induction motor used for the finite element simulations.

Corresponding author: Onwe Peter Daffin
peteronwe@unical.edu.ng
Department of Electrical and Electronic Engineering, University of Calabar, Nigeria.

JOURNAL OF SCIENCE TECHNOLOGY AND EDUCATION 14(3), SEPTEMBER, 2026
E-ISSN: 3093-0898, PRINT ISSN: 2277-0011; Journal homepage: www.atbufstejoste.com

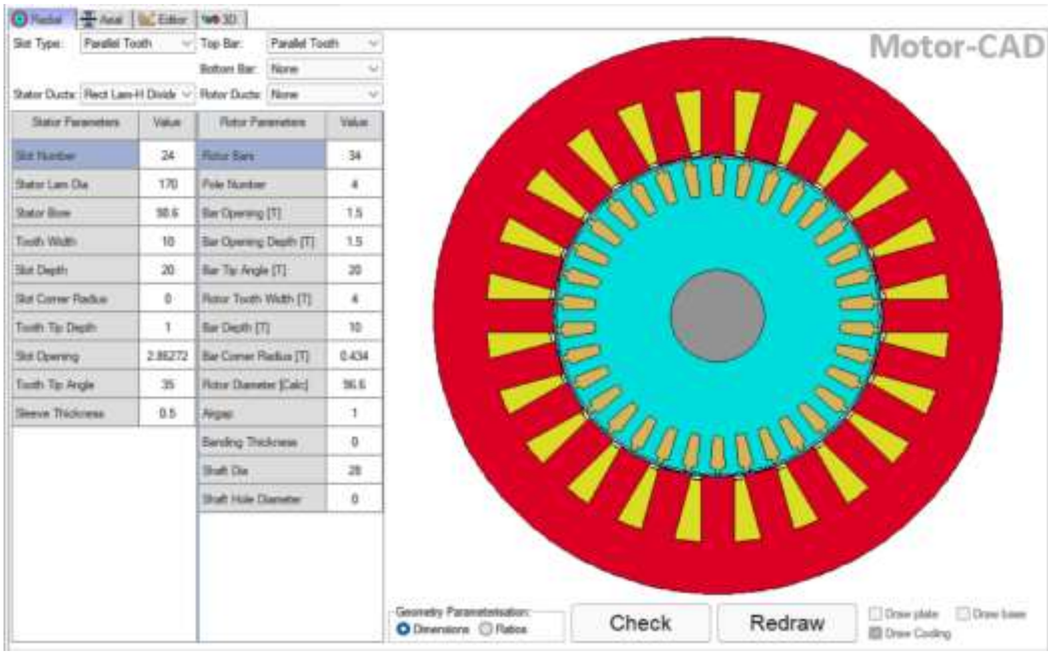

Figure 4: Geometry of the induction motor

Table 2: Material properties of the induction motor

Component	Material from Database	Electrical Resistivity	Temp Coef Electrical Resistivity	Magnet Br at 20°C	Magnet Relative Permeability	Temp Coef Br	Density	Weight	Notes
Units		Ohm.m		Tesla			kg/m³	kg	
Stator Lam (Back Iron)	M350-50A	4.4E-07	0				7650	5.083	
Stator Lam (Tooth)	M350-50A	4.4E-07	0				7650	3.212	
Stator Lamination [Total]								8.295	
Armature Winding [Active]	Copper (Annealed)	1.724E-08	0.00393				8933	0.8278	
Armature EWdg [Front]	Copper (Annealed)	1.724E-08	0.00393				8933	0.7239	
Armature EWdg [Rear]	Copper (Annealed)	1.724E-08	0.00393				8933	0.7239	
Armature Winding [Total]								2.276	
Slot Wedge							1000	0.0007295	
Rotor Lam (Back Iron)	M350-50A	4.4E-07	0				7650	2.43	
Rotor Lam (Tooth)	M350-50A	4.4E-07	0				7650	1.177	
Rotor Lamination [Total]								3.607	
Rotor Cage Top Bar	Copper (Pure)	1.724E-08	0.003862				8933	0.993	
Rotor Cage Top Bar Opening	Copper (Pure)	1.724E-08	0.003862				8933	0.06166	
Rotor Cage (Front End)	Aluminium (Cast)	3.3E-08	0.00375				2950	0.1225	
Rotor Cage (Rear End)	Aluminium (Cast)	3.3E-08	0.00375				2950	0.1225	
Rotor Cage [Total]								1.3	
Stator Bore Sleeve							4000	0.1294	
Shaft [Active]							7800	0.4323	
Shaft [Front]							7800	0.3637	
Shaft [Rear]							7800	0.2489	
Shaft [Total]								1.045	
Total Weight								16.65	Weight [Total]

EXPERIMENTAL METHOD

Experimental setup

Measurements were taken from the three-phase induction motor and compared with the finite element results. The test setup included a three-phase power supply, three-phase variac, protection and distribution unit, measuring instruments, the induction motor, loading machine, tachometer, and infrared thermometer.

An oscilloscope was used to check the voltage waveform, while the motor current was measured with the available current measuring instrument. The motor speed was measured with an infrared tachometer, and an infrared thermometer was used to measure temperature.

Corresponding author: Onwe Peter Daffin
peteronwe@unical.edu.ng
Department of Electrical and Electronic Engineering, University of Calabar, Nigeria.

The motor was tested at 380 V, which was the rated supply voltage, and the measurements obtained at this voltage were used to compare the experimental results with the rated-load simulation.

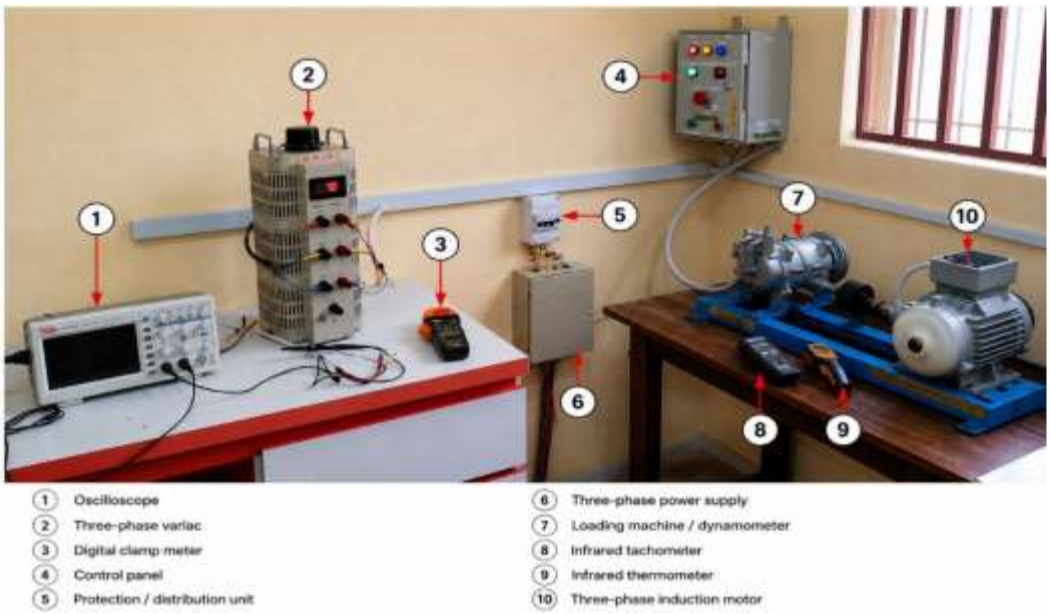

Plate1: Experimental setup

Rated-load measurement

At the rated supply voltage of 380 V, the measured phase currents were:

Table 3: Experimental measurement of the motor at rated load

S/No	Description	Values	Unit
1	Phase A current	3.70	Amps
2	Phase B current	3.68	Amps
3	Phase C current	3.86	Amps
4	Average current	3.75	Amps
5	Speed	1427	rpm

These measurements were used directly for comparison with the corresponding Motor-CAD results.

RESULTS AND DISCUSSION

Steady-state simulation results

The principal steady-state simulation results obtained from Motor-CAD are presented in Table 6.

Table 4: Steady-state simulation results at rated load

S/No	Description	Values	Units
1	Phase A rms current	3.734	A
2	Phase B rms current	3.737	A
3	Phase C rms current	3.743	A
4	Average current	3.738	A
5	Phase A peak current	5.503	A
6	Phase B peak current	5.518	A
7	Phase C peak current	5.533	A
8	Electromagnetic Torque	10.014	N/M
9	Speed	1429	RPM

Corresponding author: Onwe Peter Daffin
peteronwe@unical.edu.ng
Department of Electrical and Electronic Engineering, University of Calabar, Nigeria.

JOURNAL OF SCIENCE TECHNOLOGY AND EDUCATION 14(3), SEPTEMBER, 2026
E-ISSN: 3093-0898, PRINT ISSN: 2277-0011; Journal homepage: www.atbufstejoste.com

The simulated currents are closely balanced, with only small differences among the three phases. The average RMS current is 3.738 A, which is close to the motor's specified rated current of 3.83 A. The electromagnetic torque of 10.014 Nm is also consistent with the torque expected from a 1.5 kW motor operating close to its rated speed.

During starting, the stator currents exhibit relatively large amplitudes because the rotor is initially stationary and the motor draws a high starting current. As the rotor accelerates, the current amplitude decreases and the waveforms approach their steady-state values. The Phase A current reaches approximately ±16 A during the starting interval before reducing toward its steady-state value.

Three-phase stator currents

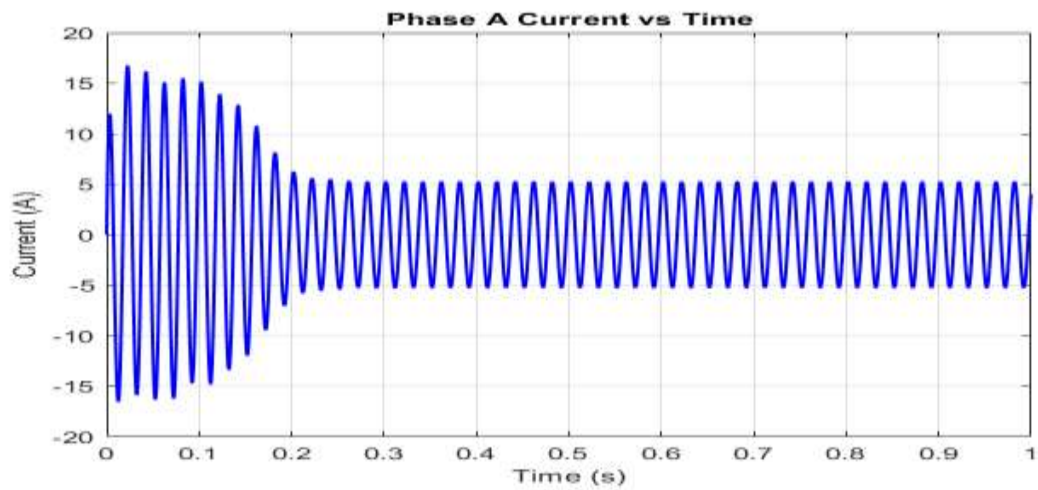

Figure 5: Graph of phase A current against time at rated load

Phase B exhibits a similar transient response, with a starting current amplitude of approximately ±17 A followed by a reduction as the motor accelerates.

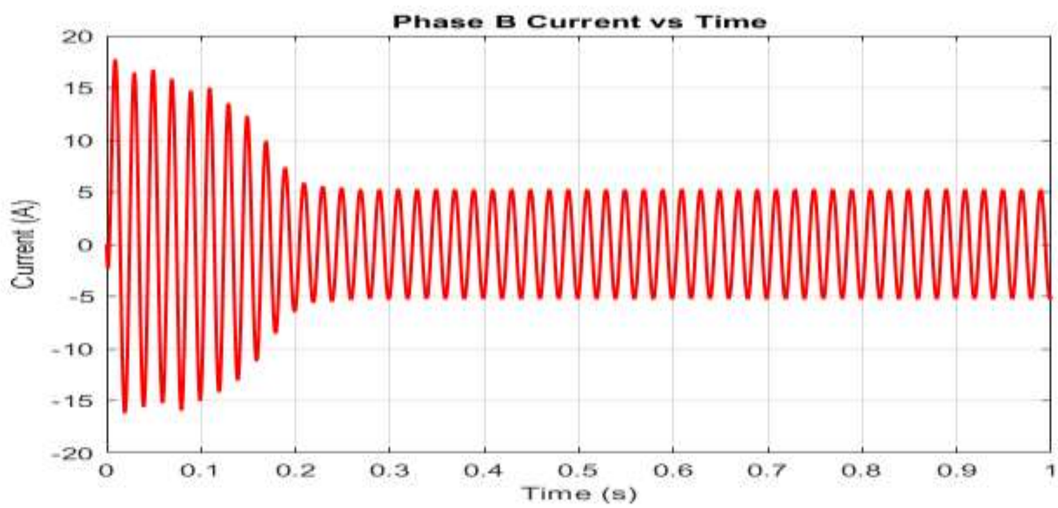

Figure 6: Graph of phase B current against time at rated load

Corresponding author: Onwe Peter Daffin
peteronwe@unical.edu.ng
Department of Electrical and Electronic Engineering, University of Calabar, Nigeria.

Phase C follows the same general pattern, with a starting current amplitude of approximately ±16 A and subsequent stabilization.

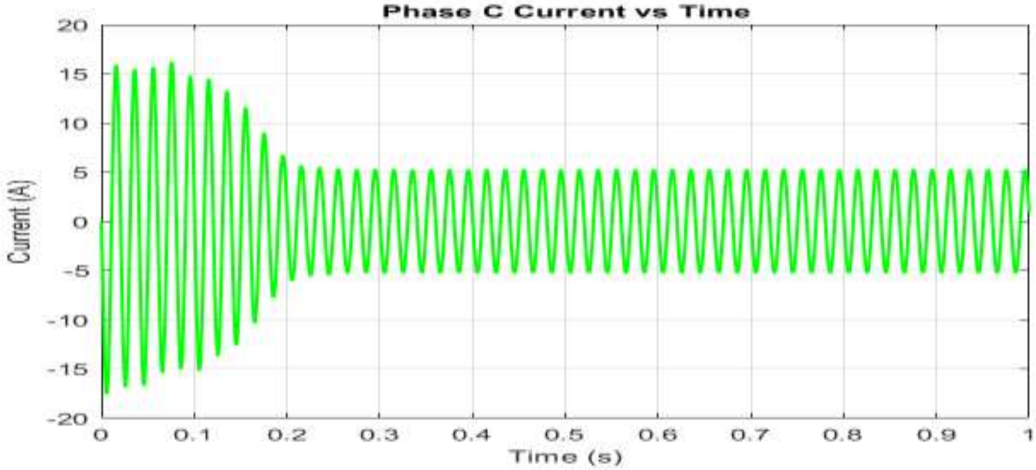

Figure 7: Graph of phase C current against time at rated load

The close similarity among the three phase currents indicates that the simulated motor operates in a substantially balanced condition at rated load. The high initial current results from the large slip at standstill. As the rotor accelerates, slip decreases, reducing the rotor-induced current and consequently the stator current toward its steady-state value.

Electromagnetic torque

The simulated electromagnetic torque exhibits a transient response during starting. At the beginning of the simulation, the motor develops a relatively high torque of approximately 16 Nm to accelerate the rotor. As the rotor speed increases, the torque oscillations reduce and the torque approaches approximately 10 Nm at steady state.

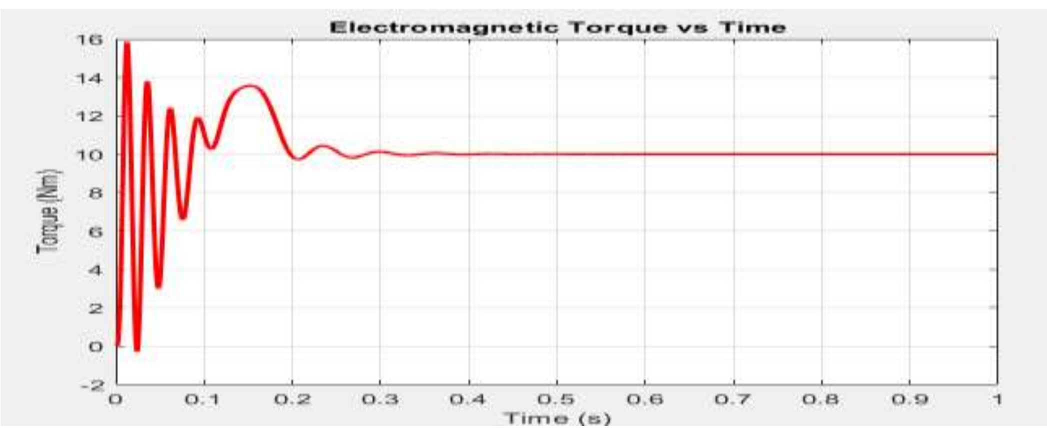

Figure 8: Graph of electromagnetic torque against time at rated load

The steady-state electromagnetic torque obtained from the simulation is 10.014 Nm. This value is consistent with the mechanical torque expected from a 1.5 kW motor operating near its rated speed. The initial torque peak is associated with the high slip condition during

Corresponding author: Onwe Peter Daffin
peteronwe@unical.edu.ng
Department of Electrical and Electronic Engineering, University of Calabar, Nigeria.

JOURNAL OF SCIENCE TECHNOLOGY AND EDUCATION 14(3), SEPTEMBER, 2026
E-ISSN: 3093-0898, PRINT ISSN: 2277-0011; Journal homepage: www.atbufstejoste.com

starting, while the subsequent reduction results from the reduction in slip as rotor speed approaches its steady-state value.

Speed response

The simulated rotor speed increased rapidly from standstill and approached a steady-state value of 1429 rpm under rated-load operation. For the four-pole, 50 Hz induction motor, the synchronous speed is 1500 rpm. Consequently, the steady-state simulated slip was calculated as 0.0473, corresponding to 4.73%. The experimental speed of 1427 rpm corresponds to a slip of 0.0487 or 4.87%. The difference between the rotor and synchronous speeds is expected in an induction motor because relative motion between the rotating magnetic field and rotor is necessary to induce rotor current and sustain electromagnetic torque. The close values of the simulated and experimental slip further demonstrate the good agreement between the numerical model and the physical motor.

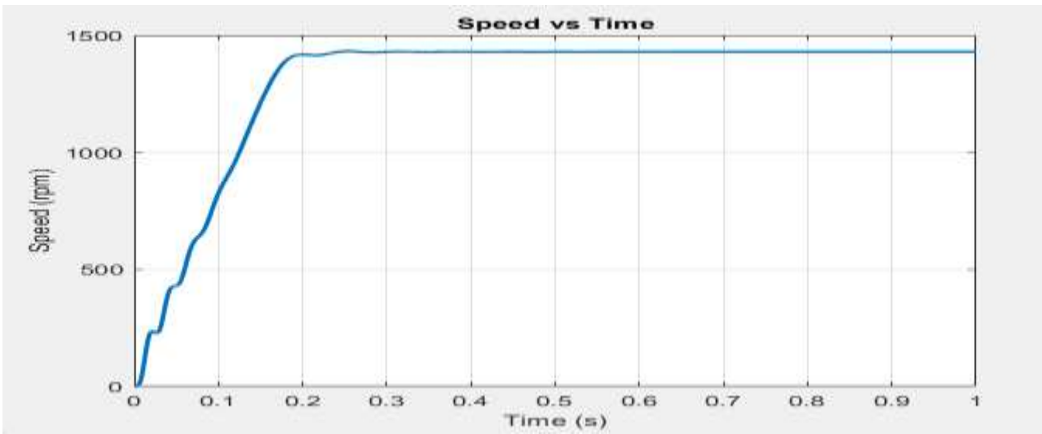

Figure 9: Graph of speed against time at rated load

Torque-speed characteristic

The torque-speed characteristic shows that the motor develops a relatively high torque during starting and that the torque decreases as the rotor accelerates toward its steady-state operating speed. The starting torque is approximately 16 Nm, while the torque approaches approximately 10 Nm near the operating point.

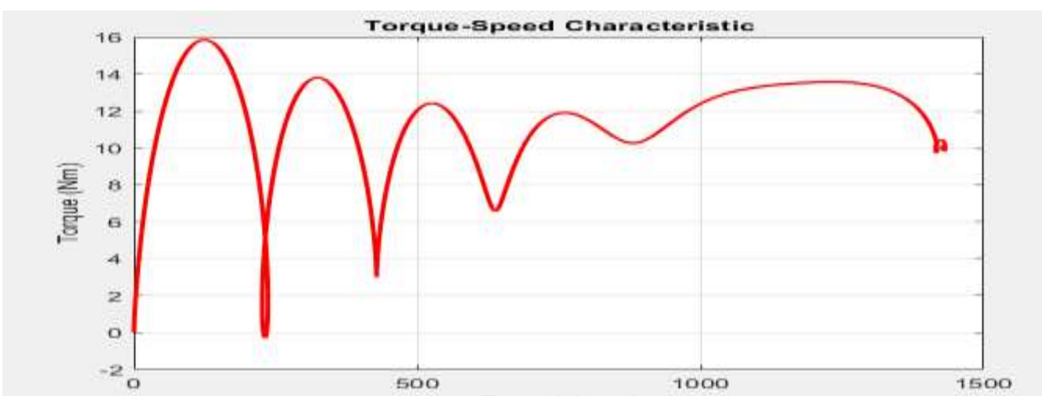

Figure 10: Graph of electromagnetic torque against speed at rated load

Corresponding author: Onwe Peter Daffin
peteronwe@unical.edu.ng
Department of Electrical and Electronic Engineering, University of Calabar, Nigeria.

JOURNAL OF SCIENCE TECHNOLOGY AND EDUCATION 14(3), SEPTEMBER, 2026
E-ISSN: 3093-0898, PRINT ISSN: 2277-0011; Journal homepage: www.atbufstejoste.com

This behaviour is characteristic of a squirrel-cage induction motor. The relatively high starting torque provides the torque required to accelerate the rotor and overcome the combined effects of inertia, applied load, and mechanical losses.

Efficiency

The simulated efficiency rises as the motor speeds up from standstill. At low speed, the motor losses are relatively high compared with the useful output, so the efficiency is lower. As the motor gets closer to its normal operating speed, the efficiency improves.

Figure 11: Graph of efficiency against speed at rated load only

The reported simulation results indicate a maximum efficiency of approximately **68%** in the region of 1400–1450 rpm.

Power factor

The power factor is relatively low during starting because the motor draws a substantial magnetizing current. As the motor accelerates and approaches its normal operating condition, the power factor improves. The simulated power factor reaches approximately 0.86 in the normal operating region.

Figure 12: Graph of power factor against speed at rated load only

Corresponding author: Onwe Peter Daffin
peteronwe@unical.edu.ng
Department of Electrical and Electronic Engineering, University of Calabar, Nigeria.

JOURNAL OF SCIENCE TECHNOLOGY AND EDUCATION 14(3), SEPTEMBER, 2026
E-ISSN: 3093-0898, PRINT ISSN: 2277-0011; Journal homepage: www.atbufstejoste.com

This improvement indicates that the proportion of the supply current contributing to useful active power becomes greater as the motor approaches its rated operating condition.

Experimental Validation

The experimental and simulated results at 380 V are compared in Table 3.

Table 5: steady-state comparison of experimental and simulated results at rated load

S/No	Parameters	Experimental results	Simulated results	Percentage Difference
1	Phase A rms current	3.7A	3.734A	0.92%
2	Phase B rms current	3.68A	3.737A	1.55%
3	Phase C rms current	3.86A	3.743A	3.03%
4	Speed	1427 rpm	1430 rpm	0.21%
5	Rated voltage	380V	380V	0

The measured and simulated values are generally close, particularly for the phase currents and speed. The largest difference among the three phase currents is 3.03%, occurring in Phase C. The speed difference is only 0.21%, indicating a very close agreement between the simulated and measured operating speeds. The voltage was identical in both cases.

DISCUSSION OF FINDINGS

The results demonstrate that the developed Motor-CAD finite element model reproduces the principal rated-load characteristics of the 1.5 kW induction motor with good accuracy. The three simulated phase currents are closely balanced, with an average RMS value of 3.738 A. This is close to the specified rated current of 3.83 A. The electromagnetic torque reaches approximately 10 Nm at steady state, which is consistent with the torque required to deliver approximately 1.5 kW at a speed close to 1430 rpm. The speed response demonstrates rapid acceleration followed by stabilization near the steady-state operating point. The transient torque is higher than the steady-state torque because additional torque is required to accelerate the rotor according to the mechanical motion equation.

The experimental validation provides further support for the finite element model. The differences in phase currents are below 4%, while the difference in speed is only 0.21%. Such agreement indicates that the model captures the major electromagnetic characteristics of the physical machine under the selected rated-load condition. The results are consistent with previous investigations showing that finite element methods can provide useful predictions of induction motor performance [1], [14]. They also support the use of numerical modelling as a complementary tool to experimental testing for induction motor performance assessment.

CONCLUSION

A 1.5 kW three-phase squirrel-cage induction motor was modelled in ANSYS Motor-CAD and tested at rated load. The simulation gave balanced phase currents, with a starting torque of about 16 Nm and a steady-state electromagnetic torque of about 10 Nm. The motor speed increased from standstill and settled at approximately 1429 rpm. The simulated efficiency was about 68%, while the power factor was approximately 0.86.

At the rated supply voltage of 380 V, the measured phase currents were 3.70 A, 3.68 A, and 3.86 A, with a measured speed of 1427 rpm. The corresponding simulated currents were 3.734 A, 3.737 A, and 3.743 A, with a speed of about 1430 rpm. The differences between the measured and simulated currents were 0.92%, 1.55%, and 3.03%, respectively, while the difference in speed was 0.21%. The small differences between the measured and simulated results show that the Motor-CAD model gives a reasonable representation of the motor's performance at rated load. The results also show that Motor-CAD, together with MATLAB for processing the simulation data, can be used to study the rated-load performance of the three-phase squirrel-cage induction motor.

Corresponding author: Onwe Peter Daffin
peteronwe@unical.edu.ng
Department of Electrical and Electronic Engineering, University of Calabar, Nigeria.

JOURNAL OF SCIENCE TECHNOLOGY AND EDUCATION 14(3), SEPTEMBER, 2026
E-ISSN: 3093-0898, PRINT ISSN: 2277-0011; Journal homepage: www.atbufstejoste.com

REFERENCES

[1] E. C. Abunike, O. I. Okoro, and G. D. Umoh, "Steady and dynamic states analysis of induction motor: FEA approach," *Nigerian Journal of Technology*, vol. 36, no. 4, pp. 1202–1207, 2017, doi: 10.4314/njt.v36i4.29.

[2] E. E. Okpo, O. I. Okoro, C. C. Awah, and U. B. Akuru, "Performance evaluation of 5.5 kW six-phase asynchronous motor," in *Proc. IEEE PES/IAS PowerAfrica Conf.*, 2019.

[3] U. O. Innocent, I. E. Nkan, E. E. Okpo, and O. I. Okoro, "Predicting the stability behaviour of three horse-power induction motor using eigenvalue method," *Bayero Journal of Engineering and Technology*, vol. 16, no. 2, pp. 66–81, 2021.

[4] E. J. Akpama and L. U. Anih, "Modelling and simulation of multiphase induction machine," *International Journal of Engineering Innovation & Research*, vol. 4, no. 5, pp. 732–737, 2024.

[5] E. J. Akpama, O. I. Okoro, and E. Chikuni, "Simulation of the performance of induction machine under unbalanced source voltage conditions," *Pacific Journal of Science and Technology*, vol. 11, no. 1, pp. 9–15, 2010.

[6] E. J. Akpama, I. E. Omini, E. E. Effiong, and R. U. Ezenwosu, "PID speed controlled model of induction motor using Simulink," *International Journal of Engineering Research and Management*, vol. 7, no. 10, pp. 24–28, 2020.

[7] A. O. Inope, D. C. Idoniboyeobu, and S. L. Braide, "Performance analysis of starting and control effect of three-phase induction motors," *Global Scientific Journal*, 2022.

[8] P. D. Onwe, E. J. Akpama, O. I. Okoro, and O. Ekpenyong, "Dynamic behavior of asynchronous motor under balanced and unbalanced voltage source conditions," *World Journal of Engineering Research and Technology*, vol. 11, no. 4, pp. 239–252, 2025.

[9] O. I. Okoro, "MATLAB simulation of induction machine with saturation leakage and magnetizing inductances," *Pacific Journal of Science and Technology*, vol. 5, no. 1.

[10] I. Boldea, *Induction Machines Handbook*. Boca Raton, FL, USA: CRC Press, 2020.

[11] S. J. Chapman, *Electric Machinery Fundamentals*, 5th ed. New York, NY, USA: McGraw-Hill, 2012.

[12] P. C. Krause, O. Wasynczuk, S. D. Sudhoff, and S. Pekarek, *Analysis of Electric Machinery and Drive Systems*, 3rd ed. Hoboken, NJ, USA: Wiley-IEEE Press, 2013.

[13] J. Pyrhönen, T. Jokinen, and V. Hrabovcová, *Design of Rotating Electrical Machines*, 2nd ed. Chichester, U.K.: Wiley, 2014.

[14] M. Deshmukh, P. B. Daigavane, and S. P. Gawande, "Performance analysis of three-phase squirrel-cage induction motor using finite element method," *International Journal of Engineering Research and Applications*, vol. 7, no. 6, pp. 45–52, 2017.

[15] P. Sharma, R. Singh, and A. Kumar, "Review of three-phase induction motor performance and applications," *International Journal of Scientific and Technology Research*, vol. 9, no. 4, pp. 456–462, 2020.

Corresponding author: Onwe Peter Daffin
peteronwe@unical.edu.ng
Department of Electrical and Electronic Engineering, University of Calabar, Nigeria.